

# Thermal Stimulation of the Retina Reduces Bruch's Membrane Thickness in Age Related Macular Degeneration Mouse Models

Jan Tode<sup>1,\*</sup>, Elisabeth Richert<sup>1,\*</sup>, Stefan Koinzer<sup>1</sup>, Alexa Klettner<sup>1</sup>, Claus von der Burchard<sup>1</sup>, Ralf Brinkmann<sup>2</sup>, Ralph Lucius<sup>3</sup>, and Johann Roeder<sup>1</sup>

<sup>1</sup> Christian-Albrechts-University of Kiel, University Medical Center, Department of Ophthalmology, Kiel, Germany

<sup>2</sup> Institute for Biomedical Optics, University of Lübeck, and Medical Laser Center Lübeck GmbH, Lübeck, Germany

<sup>3</sup> Christian-Albrechts-University of Kiel, Institute of Anatomy, Kiel, Germany

**Correspondence:** Jan Tode, Christian-Albrechts-University of Kiel, University Medical Center, Department of Ophthalmology, Arnold-Heller-St 3, 24105 Kiel, Germany. e-mail: jan.tode@uksh.de

**Received:** 5 September 2017

**Accepted:** 16 March 2018

**Published:** 1 May 2018

**Keywords:** thermal stimulation of the retina (TS-R); nondamaging retinal laser therapy (NRT); sub-threshold laser therapy; age related macular degeneration (AMD); Bruch's membrane; drusen

**Citation:** Tode J, Richert E, Koinzer S, Klettner A, von der Burchard C, Brinkmann R, Lucius R, Roeder J. Thermal stimulation of the retina reduces Bruch's membrane thickness in age related macular degeneration mouse models. *Trans Vis Sci Tech.* 2018;7(3):2, <https://doi.org/10.1167/tvst.7.3.2>  
Copyright 2018 The Authors

**Purpose:** To investigate the effect of thermal stimulation of the retina (TS-R) on Bruch's membrane (BrM) thickness in age-related macular degeneration (AMD) mouse models as a novel concept for the prophylaxis and treatment of dry AMD.

**Methods:** Two knockout AMD mouse models, B6.129P2-ApoE<sup>tm1Unc</sup>/J (ApoE<sup>-/-</sup>) and B6.129X1-Nfe2l2<sup>tm1Ywk</sup>/J (NRF2<sup>-/-</sup>), were chosen. One randomized eye of each mouse in four different groups (two of different age, two of different genotype) of five mice was treated by TS-R (532 nm, 10-ms duration, 50- $\mu$ m spot size), the fellow eye served as control. Laser power was titrated to barely visible laser burns, then reduced by 70% to guarantee for thermal elevation without damage to the neuroretina, then applied uniformly to the murine retina. Fundus, optical coherence tomography (OCT), and fluorescein angiography (FLA) images were obtained at the day of treatment and 1 month after treatment. Eyes were enucleated thereafter to analyze BrM thickness by transmission electron microscopy (TEM) in a standardized blinded manner.

**Results:** Fundus images revealed that all ApoE<sup>-/-</sup> and NRF2<sup>-/-</sup> mice had AMD associated retinal alterations. BrM thickness was increased in untreated controls of both mouse models. Subvisible TS-R laser spots were not detectable by fundus imaging, OCT, or FLA 2 hours or 1 month after laser treatment. TEM revealed a significant reduction of BrM thickness in laser-treated eyes of all four groups compared to their fellow control eyes.

**Conclusions:** TS-R reduces BrM thickness in AMD mouse models ApoE<sup>-/-</sup> and NRF2<sup>-/-</sup> without damage to the neuroretina. It may become a prophylactic or even therapeutic treatment option for dry AMD.

**Translational Relevance:** TS-R may become a prophylactic or even therapeutic treatment option for dry AMD.

## Introduction

Age-related macular degeneration (AMD) is a progressive degenerative disease of choroid, Bruch's membrane (BrM), retinal pigmented epithelium (RPE), and neuroretina. It commences after the age of 50. In the industrialized world, early stage AMD affects one-third of the population at 75 years of age or older—advanced AMD more than 7% of the population at that age.<sup>1</sup> AMD is the cause of

approximately 50% of severe visual impairment and the most common cause for legal blindness of the elderly in the developed world.<sup>2</sup> The need for early and prophylactic AMD therapies to prevent the occurrence of advanced AMD, often followed by legal blindness, is unmet.

AMD can be divided into two different forms, the slowly progressive nonexudative (dry) form and the fast-progressive exudative (wet) form. Dry AMD is characterized by alterations of the RPE leading to

pigment clumping and by metabolic deposits within the RPE-BrM-complex called drusen.<sup>3</sup> Dry AMD may develop to an advanced stage characterized by RPE- and neuroretinal atrophy or it may evolve to wet AMD, which leads to legal blindness quickly in its natural course. Wet AMD is characterized by the appearance of pathological neovascularization of the choroid.<sup>4</sup>

The multifactorial pathology of AMD is not entirely understood. Besides age, genetic variations involving, for example, complement factor H (CFH), complement factor I (CFI), tissue inhibitor of matrix metalloproteases (TIMP3)<sup>5</sup> and factors like high caloric nutrition, lack of physical exercise, oxidative stress, and smoking<sup>6</sup> have been shown to promote AMD. The current concept of the underlying molecular mechanisms of AMD is based on four assumptions: impairment of lipid metabolism, extracellular matrix modifications, inflammatory processes, and altered angiogenesis.

Lipid metabolism of the RPE is essential to provide sufficient nutrients and phospholipids consumed by photoreceptors. The metabolism of lipophilic substances leads to an accumulation of esterified cholesterol within the RPE, which is recomposed with apolipoprotein (Apo) B produced by the RPE itself. ApoB containing high density lipoprotein (HDL) like lipoproteins are excreted basolaterally to BrM and under physiological conditions absorbed by choroid capillary plasma. In AMD, this metabolic pathway is impaired and lipophilic metabolites accumulate in the RPE-BrM-complex.<sup>7</sup>

The multilayered BrM is composed of extracellular matrix and represents the compound basement membranes of RPE and choriocapillaris. It moderates the exchange of nutrients and gas between the choroid and RPE. The homeostasis of this collagenous mesh is mediated by matrix metalloproteases (MMP) and their antagonists tissue inhibitors of metalloproteases (TIMP) secreted mainly by the RPE and to a lesser extent by endothelial cells of the choroid.<sup>8-11</sup> In AMD, the homeostatic processes of degradation and rebuilding of BrM are malfunctioning. This leads to an increase in BrM thickness enhanced by metabolic deposits.

Deposits within the RPE-BrM-complex and extracellular matrix modifications under the influence of oxidative stress or genetic predisposition (e.g., malfunction of the complement regulator CFH) may trigger inflammatory processes.<sup>12-14</sup> Homeostatic para-inflammatory mechanisms are abandoned in AMD and features of inflammation become evident.

Components of the complement system, inflammatory cytokines (interleukin [IL]-6, tumor necrosis factor [TNF]- $\alpha$ ), macrophages, neutrophils, and other immune cells can be found within and around BrM<sup>14-17</sup> and especially in drusen.<sup>18</sup> Parts of the innate immune system as well as external factors lead to an increase in oxidative stress and thereby to oxidation of the abundant lipids in and around BrM forming, for example,  $\omega$ -(2-carboxyethyl)pyrrole (CEP).<sup>19</sup>

Under physiological conditions angiogenesis underlies a homeostasis of pro- and antiangiogenic factors. In AMD, the RPE is stressed by malnutrition and hypoxia deriving from a thickened BrM that inhibits nutrient and gas exchange. Additionally, the RPE is stressed by oxidative processes and stimulated by proinflammatory cytokines. All of this is leading to an increased expression of vascular endothelial growth factor (VEGF), evoking vessel growth originating from the choroid.<sup>20-22</sup>

In summary, one of the main features of AMD is a pathologically thickened BrM. A therapeutic means to reduce BrM thickness could therefore be a promising option to cure early stages of AMD and prevent disease progression. To date, there is no effective treatment that addresses early AMD-related mechanisms with a preventive approach.

Laser irradiation of the retina has various effects on RPE and neuroretina. Former studies have shown that laser photocoagulation of patients with early AMD aimed on drusen may lead to degradation of these metabolic deposits. However, this method has no influence on visual outcome and does not alter disease progression.<sup>23</sup> One of the main reasons for the therapeutic failure of supra-threshold laser photocoagulation for the treatment of AMD is retinal necrosis.<sup>23-25</sup> The anatomical region of pathological processes in patients with AMD is the macula and there especially the fovea region. Supra-threshold laser photocoagulation is prohibited in the fovea region, since thermal necrosis of the fovea would lead to irreversible vision loss or even legal blindness. Since supra-threshold laser photocoagulation is no option for the treatment of early AMD, sub-threshold laser therapy has been of recent interest.

The photomechanical selective retina therapy (SRT) and retinal rejuvenation therapy (2RT<sup>TM</sup>), as well as the photothermal transpupillary thermotherapy (TTT) and thermal stimulation laser therapies (like thermal stimulation of the retina [TS-R] and nondamaging retinal laser therapy [NRT]), are the known laser treatment modalities that neither affect neuroretinal anatomy nor function.

SRT<sup>26–29</sup> uses a train of microsecond laser pulses that leads to the formation of microbubbles at the intracellular RPE melanosomes, causing a selective disruption of RPE cell membranes.<sup>30,31</sup> RPE cell death is followed by migration and proliferation of the remaining RPE cells until the RPE monolayer is restored.<sup>26,32</sup> SRT has shown therapeutic effect on central serous chorioretinopathy and diabetic macular edema, as well as other entities that lead to the formation of subretinal fluid or retinal edema in clinical pilot trials.<sup>27,33</sup> SRT is not investigated here.

2RT<sup>™</sup> is a nanopulse laser technology that leads to RPE cell death, unevenly distributed within the laser spot, without damage to the neuroretina.<sup>34</sup> It has been shown that 2RT<sup>™</sup> may alter AMD-like alterations in the ApoE<sup>–/–</sup> model, as well as in humans<sup>35</sup> to some degree. It is currently under investigation within the scope of a phase 3 clinical trial. This laser modality is also not investigated here.

TTT is a laser modality that increases RPE temperature by the application of millimeter-wide spots with long exposures (60 seconds) to the macula.<sup>36,37</sup> It is hypothesized that it increases the temperature in the irradiated area, especially affecting dividing cells, as seen in wet AMD choroidal neovascularisation (CNV) formation, leading to a decrease of CNV as therapeutic approach. However, repeatedly observed damage to neuroretinal cells,<sup>38</sup> due to lack of power control mechanisms, TTT has not been under investigation anymore.

Thermal stimulation therapies (TS-R and NRT)<sup>39–41</sup> are continuous wave (cw) or micropulse laser thermal stimulations that lead to a sublethal temperature increase within the RPE without induction of necrosis or apoptosis in RPE or neuroretina. They have shown therapeutic effect in diabetic macular edema and central serous chorioretinopathy.<sup>39,41</sup> Our preliminary previous data have shown that TS-R induced hyperthermia influences the RPE secretion of AMD-relevant enzymes and signal proteins such as MMP, VEGF, and pigment epithelium-derived factor (PEDF) in porcine organ cultures. Active MMP-2 is upregulated, VEGF downregulated, and PEDF upregulated (Richert E, et al. under review). In vitro studies demonstrated that treatment of human BrM with activated MMPs leads to an enhancement of transport capacity.<sup>42</sup> We hypothesize that TS-R may lead to a restoration of the homeostasis of MMPs and thereby to a restoration of BrM, possibly facilitating trans-BrM metabolic exchange and RPE/photoreceptor nutrition. It might therefore be a therapeutic option for dry AMD.

To test this hypothesis, we evaluated the effect of

TS-R on BrM thickness in two AMD mouse models where untreated fellow eyes served as controls.

Two knockout mouse models were chosen to cover the four assumptions that underlie the molecular mechanisms of AMD: impairment of lipid metabolism, remodeling of extracellular matrix, inflammatory processes, and altered angiogenesis.

Apolipoprotein E (ApoE) knockout mice have a reduced catabolism of triglycerides and low-density lipoproteins and are therefore hyperlipidemic and hyperlipoproteinemic. Lipids are known to accumulate in blood vessels and in BrM in these animals leading to an increase in BrM thickness and remodeling of its structure. This strain is known to show AMD-like alterations of the Choroid/BrM/RPE Complex from 2 months of age.<sup>43</sup>

Nuclear factor E2-related factor 2 (Nrf2) knockout mice, on the other hand, lack one of the most important transcription factors of antioxidative processes. Antioxidant response elements (AREs) and drug metabolizing enzymes (DMEs) are downregulated in these mice leading to an increase in cellular stress and accumulation of oxidized cell metabolism products within the RPE and in BrM. This leads to secondary RPE degeneration, inflammatory processes, BrM thickening, and in elderly mice CNV formation.<sup>44</sup> AMD-like alterations have been described from 9 months of age.

## Methods

### AMD Mouse Models

Both knockout strains (ApoE<sup>–/–</sup> and NRF2<sup>–/–</sup>) were purchased from the Jackson Laboratories (Bar Harbor, ME) and housed and bred at the local university animal care unit. The homozygous genotype was confirmed by polymerase chain reaction (PCR) from tail clips. The wild type C57BL6/J control mice were obtained from the local animal care facility. Mice were kept on a regular 12-hour night and day cycle and fed standard murine diet and water ad libitum. All animal experiments were conducted in accordance to the EU directive 2010/63/EU for animal experiments. They were approved by the animal ethics and welfare committee (approval number: V 242-7224.121-12 [61-5/14]) located at the ministry of energy transition, agriculture, environment, and rural areas in Schleswig-Holstein according to German federal and European law. Animal experiments adhere to the ARVO Statement for the Use of Animals in Ophthalmic and Vision Research.

## Animal Maintenance and Anesthesia During Experiments

All examinations and laser treatment were conducted under general anesthesia. Deep anesthesia was induced by an intraperitoneal injection of a mixture of 0.05 mg/kg body weight fentanyl (Braun, Melsungen, Germany), 5.0 mg/kg body weight midazolam (Hameln Pharma, Hameln, Germany), and 0.5 mg/kg body weight medetomidine (CP-Pharma, Bergdorf, Germany).

The animal was then placed on a rigid examination platform, and body temperature was maintained within normal limits using a heating mat. Pupils were dilated by 0.025 mg/mL phenylephrine and 0.05 g/mL tropicamide (UKSH Pharmacy, Kiel, Germany), and eyes were covered with a protective moisturizing gel (2% Methylcellulosis Methocel®, Puchheim, Germany). After each examination, the anesthesia was antagonized by a mixture of 1.2 mg/kg body weight naloxone (Braun), 0.5 mg/kg body weight flumazenil (Inresa GmbH, Freiburg, Germany), and 2.5 mg/kg body weight atipamezole (Orion Pharma, Espoo, Finland). Anesthesia was uneventful in all mice. Animal wellbeing was evaluated by a standard score sheet and was uneventful in all included mice. After the final examination, animals were euthanized by cervical dislocation at the day of enucleation under deep anesthesia.

## Examinations

All examinations were conducted under general anesthesia. All mice were examined by funduscopy using a contact fundus camera (MICRON III, Phoenix Research Labs, Pleasanton, CA). The integrity of the retina was assessed, the number of drusen-like retinal spots (DRS) was counted, RPE atrophy evaluated, and CNV noted.

Optical coherence tomography (OCT) (small animal OCT, Thorlabs, Lübeck, Germany) was applied via contact optics to evaluate the retinal structure, confirm retinal integrity after laser treatment, and to confirm CNV. After laser treatment, it was used to investigate anatomical integrity of retinal layers.

Fluorescein (10% Fluorescein, 60 mg/kg body weight in 100  $\mu$ L saline intraperitoneally; Alcon Pharma, Freiburg, Germany) angiography (FLA) (MICRON III) was performed after laser treatment to evaluate vessel integrity, to detect vessel leakage, and to confirm possible CNV formation.

All examinations were repeated at the day of enucleation, thus 1 month after laser treatment.

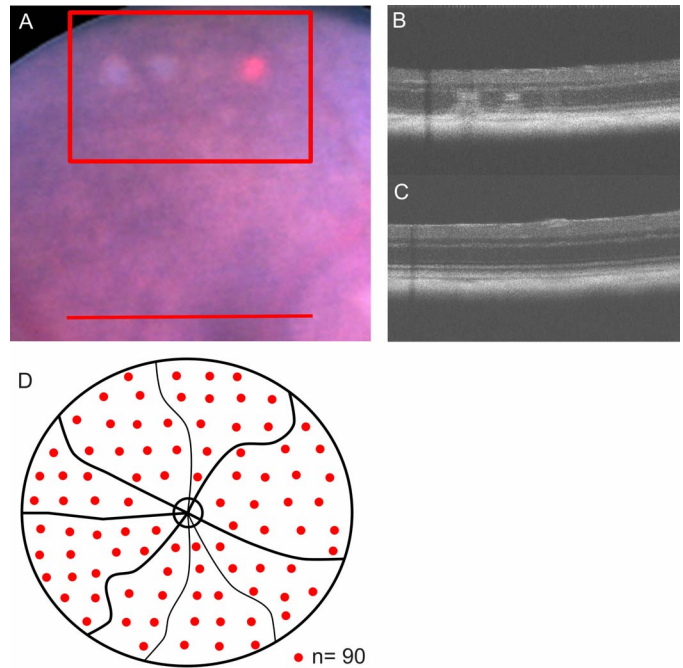


**Figure 1.** Laser spot titration and distribution. (A) Laser spots were titrated in the peripheral murine retina (red box) starting from above threshold (from left to right: first white burn) to barely visible lesions (third barely visible burn). The red spot is the aiming beam. TS-R laser treatment was carried out further centrally (red line). All treatment spots were funduscopically invisible. In OCT images, titration lesions were visible (B), and TS-R treated areas showed no anatomical alterations in OCT (C). TS-R treatment spots were distributed uniformly across an optic nerve centered approximately 50° field of view at two-spot interspot spacing, sparing optic nerve disc and retinal vessels (D).

## Laser Treatment

For TS-R a frequency doubled Neodym-Vanadate-Laser (Nd:VO<sub>4</sub>) experimental laser (Carl Zeiss Meditec AG, Jena, Germany) with a wavelength of 532 nm was used. The light was coupled to an optical multimode fiber of square cross section with a 70 × 70  $\mu$ m<sup>2</sup> core profile. The laser light was applied via contact laser-injector (Phoenix Research Labs) attached to the MICRON III camera. The pilot laser was controlled visually via MICRON III live fundus imaging.

Spot size was determined by the size of the laser fiber and laser injector, fixed to 50  $\mu$ m and could not be changed in size. Duration of irradiation was fixed to 10 ms. The intended stimulating effect was titrated visually by decreasing power at the peripheral retina from a clearly visible white burn at higher power to a barely visible spot at lower power (see Fig. 1). The barely visible burn was classified threshold. Power

was reduced by 70% to determine stimulating laser power similar to the work of Lavinsky and Palanker.<sup>40</sup> Laser spots were distributed uniformly across the retina at two spots interspot spacing to an optic disc centered approximately 50° field of view. No laser spot was aimed on vasculature.

## Transmission Electron Microscopy (TEM)

Enucleated murine eyes were fixated in 4% glutaraldehyde (Merck, Darmstadt, Germany) for 24 hours. Afterwards, the anterior segment was removed under stereomicroscopic (Stemi SV6, Carl Zeiss Meditec AG) control. The posterior eye cup was then embedded into araldite as follows: it was watered in phosphate-buffered saline (PBS; Serva, Heidelberg, Germany) overnight and put into 2% osmium tetroxide (Merck) for 2 hours the next day. Afterwards, eyes were dehydrated in increasing ethanol series at room temperature (70% for 30 minutes, 80% for 40 minutes, 90% and 99% for 50 minutes) and then incubated in propylenoxide (Merck) 2 × 10 minutes each. A mixture of 91 mL araldite-M (Sigma, Steinheim, Germany) and 84 mL dodeceny succinic anhydride (epoxy embedding medium hardener; Sigma) was augmented by 3% araldite M accelerator (Sigma). This mixture was stirred 1:1 with propylene oxide, and the eyes were placed into this medium at room temperature overnight. The next day, araldite combined with 2% araldite M accelerator was added for 4 hours. Eyes were then incubated for 2 hours at room temperature and then hardened at 48°C overnight. Next day temperature was increased to 60°C for another 48 hours.<sup>45</sup>

Araldite embedded eyes were cut by microtome to sections of 100 nm following a standardized protocol. The first set of three sections was conducted inferior to the rim of the optic nerve, the second set crossed the optic nerve, and the third set of sections was superior to the rim of the optic nerve (see Fig. 2). These sections were contrasted by lead citrate (Merck) and uranyl acetate (Merck) and then examined by TEM Zeiss EM 900 (Carl Zeiss Meditec AG). To eliminate observer bias, the calculation of BrM thickness was done in a standardized and blinded manner by a single trained biologist. From each set of three sections, the first section was examined (two sections in case of damage) taking three pictures at defined spots in proximity to grid bars anterior to the optic nerve and three pictures posterior to the optic nerve. The first picture was always taken strictly behind the first grid bar adjacent to the start of regular RPE morphology in proximity to the optic

nerve cavity (where there is no RPE). The second picture was taken strictly before the second grid bar, the third picture strictly behind the second grid bar. Three measurements per picture were carried out. Areas of intercapillary pillars were left out. In total, 54 measurements per eye determined the thickness of BrM (Fig. 2).

## Genotyping

The validity and homogeneity of the intended genotype as well as screening for retinal degeneration 8 mutation of Crumbs-homologue 1 (CRB1<sup>rd8</sup>), known to confound retinal phenotype, was determined by PCR from tail clips. According to Mehalow et al.,<sup>46</sup> for CRB1<sup>rd8</sup> the following set of primers was used: mCRB1 mF2 (5'-GCCCTGTTTGCATG GAGGAACTTGAAGACAGCTA-CAGTTCTT CTG-3'), mCRB1 mF1 (5'-GTGAAGACAGCTA CAGTTCTGATC-3'), and mCRB1 mR (5'-GCCCCATTTGCACACTGATGAC-3'). NRF2 mice had to be genotyped since breeding was more productive in homozygous NRF2<sup>-/-</sup> + heterozygous NRF2<sup>-/+</sup> mice, but only homozygous NRF<sup>-/-</sup> could be included into the study. According to manufacturer's specifications, for NRF2 the following primers were used: NRF2 c\_forward (5'-GCCTGA GAGCTGTAGGCC-3'), NRF2 Wt\_reverse (5'-GGAATGGAAAATAGCTCCTGCC-3'), and NRF2 Mut\_reverse (5'-GACAGTATCGGCC CAGGAA-3'). ApoE mice were not genotyped before experiments, because all parental mice were homozygous as specified by the vendor.

After PCR, an agarose gel electrophoresis was carried out. Since two makeups were prepared, for CRB1<sup>rd8</sup> two possible genotypes were expected: wild-type (220 base pairs) and mutant (244 base pairs). For NRF2, one makeup was prepared, hence three possible genotypes were expected: wildtype (262 base pairs), heterozygous (262 and 400 base pairs), and homozygous (400 base pairs).

## Experimental Protocol

First, the validity of the two knockout strains as representative of AMD was to be confirmed. Untreated C57BL/6J mice of 5 and 13 months of age were examined clinically (funduscopy, OCT, FLA) and by TEM. ApoE<sup>-/-</sup> of 5 and NRF2<sup>-/-</sup> of 13 months of age were also examined as untreated control. For the untreated controls both eyes were included. Then, experimental treatment groups had to be defined. From the literature, it is known that

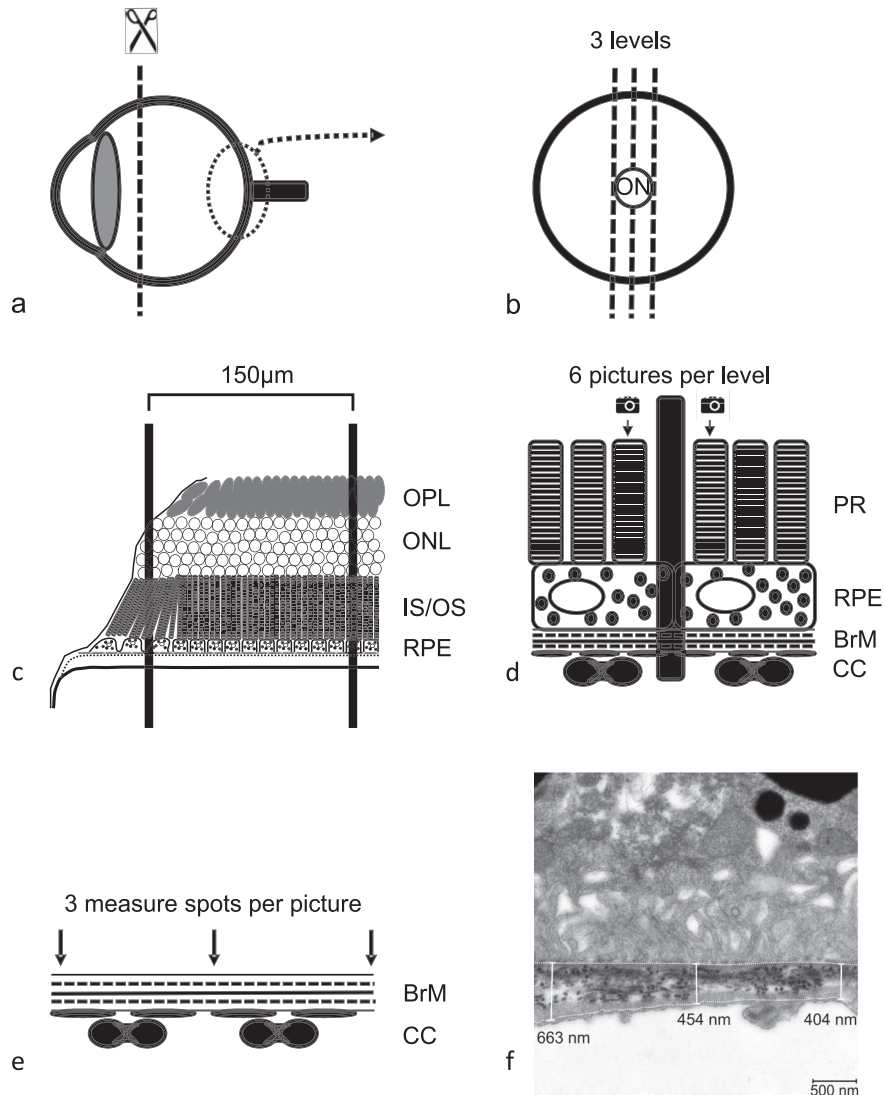


**Figure 2.** TEM. The anterior segment of the enucleated and fixated eye ball (a) was embedded in araldite and sectioned at three optic nerve disc (ON) centered levels (b). The sections were placed on a copper grid with an intergrid-distance of 150  $\mu\text{m}$ . Grid bars were counted starting from the first grid bar that covered a piece of retina that showed all outer retinal layers in the right anatomical order (the second grid bar shown in scheme c). Therefore, the maximum distance of picture one from optic disc was 300  $\mu\text{m}$ , the minimum distance 150  $\mu\text{m}$ . All pictures were taken within an optic disc centered radius of 450  $\mu\text{m}$ . Three pictures (12,000-fold magnification) to both sides of the optic nerve of each section were taken (d) always in front of the first and in front of and behind the second grid bar (*black middle bar*) generating a total of six pictures per section. Within each picture, three measurements of BrM thickness were conducted (e, f). The thereby determined BrM thickness is a result of 54 measurements per eye. An overview picture (3000-fold magnification) of each level was taken to examine ultrastructural integrity of RPE before BrM thickness was measured in higher magnification.

ApoE<sup>-/-</sup> mice from the age of 2 months and most ApoE<sup>-/-</sup> mice at the age of 8 months, as well as NRF2<sup>-/-</sup> mice from the age of 9 months and most NRF2<sup>-/-</sup> mice at the age of 12 months show AMD-like alterations of the choroid/BrM/RPE complex.<sup>43,44</sup> For both strains, an early (4 months old ApoE<sup>-/-</sup>, 9 months old NRF2<sup>-/-</sup>) and a later stage of AMD development (8 months old ApoE<sup>-/-</sup>, 12 months old NRF2<sup>-/-</sup>) was chosen. Since the treated

mice were enucleated 1 month after TS-R, at the age of 5 and 9 months for the ApoE<sup>-/-</sup>, and 10 and 13 months for the NRF2<sup>-/-</sup>, untreated controls were also chosen at comparable ages.

One randomized eye of each mouse in the four different treatment groups (two of different age, two of different strain) of five mice each was treated by TS-R; the fellow eye served as control (see Table 1).

**Table 1.** Number of Mice, Eyes, and Measurements Included in Each Group

Strain	Age, mo	Control (c) Laser (l)	Mice, <i>n</i>	Eyes, <i>n</i>	Measure, <i>n</i>
BL/6J	5	c untreated	3	6	324
BL/6J	13	c untreated	3	6	324
ApoE <sup>-/-</sup>	5	c untreated	3	6	324
NRF2 <sup>-/-</sup>	13	c untreated	3	6	324
ApoE <sup>-/-</sup>	5	c treated	5	5	270
ApoE <sup>-/-</sup>	5	l	5	5	270
ApoE <sup>-/-</sup>	9	c treated	5	5	270
ApoE <sup>-/-</sup>	9	l	5	5	270
NRF2 <sup>-/-</sup>	10	c treated	5	5	270
NRF2 <sup>-/-</sup>	10	l	5	5	270
NRF2 <sup>-/-</sup>	13	c treated	4	4	216
NRF2 <sup>-/-</sup>	13	l	4	4	216

In the NRF2<sup>-/-</sup> 13-month group, one mouse died preterm. Above, untreated controls, both eyes were included; Below, mice from laser treatment groups, untreated fellow eyes are controls.

## Statistics and Power Calculation

The primary endpoint of the study was BrM thickness. Secondary endpoints were alterations of the AMD-like phenotype and ultrastructural changes of the RPE. The comparison of the laser effect was done intraindividually. Therefore, numbers could be kept low. Since the presented data were a pilot trial with unknown effect, no power calculation was obtained beforehand. Groups of five mice each were built. Control groups were reduced to a number of three, since both eyes could be included into the determination of BrM thickness. BrM thickness was determined as the mean of 54 measurements per eye. Values were compared by paired *t*-test and exact Fisher's test, a confidence interval of 95% was chosen, and *P* values  $\leq 0.05$  were considered significant. Statistics were calculated by R (www.r-project.org).

## Results

### Description of the Model

The first question addressed the viability (s.o.) of the AMD mouse models. Clinical examinations were carried out to determine the AMD-like phenotype of the two strains. Fundus images revealed that all ApoE<sup>-/-</sup> and NRF2<sup>-/-</sup> mice had AMD associated retinal alterations like DRS and areas of hypopig-

mented RPE (see Fig. 3). OCT showed various changes in the choroid/BrM/RPE/neuroretina architecture in the vicinity of DRS and RPE hypopigmentations, associated with an AMD phenotype. Prominent DRS were seen adjacent to the RPE, mostly deferring the structure of the neuroretina (see Fig. 3). Funduscopically identified larger areas of multiple DRS, mostly appeared as gap-like alterations in the pigmented choroid layer. Presumed CNV could well be detected by OCT and was only seen in one 13-month-old NRF2<sup>-/-</sup> eye. This was confirmed by FLA.

AMD-like alterations differed depending on the genotype. They were more severe and diverse in NRF2<sup>-/-</sup> than in ApoE<sup>-/-</sup> mice. These alterations were never seen in BL/6J wild type mice. All NRF2<sup>-/-</sup> mice were homozygous NRF2 knockout and unexpectedly homozygous CRB1<sup>rd8</sup> although created on a C57BL/6J background known to be CRB1<sup>rd8</sup> negative. ApoE<sup>-/-</sup> and BL/6J wild type mice were CRB1<sup>rd8</sup> negative.

An AMD-like phenotype was not only seen in clinical examinations, but also in the ultrastructural images in TEM. Figure 4 gives examples of common alterations in TEM examinations, like deposits and vacuoles within the outer collagenous layer, loss of fenestration, and basal lamina splicing of the choroidal endothelium. These AMD-like ultrastructural changes of the choroid/BrM/RPE complex could be seen in all eyes examined.

BrM thickness was increased in both untreated control and knockout strains. Five-month-old ApoE<sup>-/-</sup> mice had a mean BrM thickness of 551 nm  $\pm$  10.4 standard error of the mean (SEM), 13-month-old NRF2<sup>-/-</sup> mice had a mean BrM thickness of 634 nm  $\pm$  16.1 SEM. This was significantly more (both *P* < 0.0001; paired *t*-test) compared to age-matched untreated wild type C57BL/6J animals of 5 months of age (mean 442 nm  $\pm$  5.4 SEM), as well as 13 months of age (mean 546 nm  $\pm$  8.9 SEM) (see Fig. 5).

### Reduction of BrM Thickness

The primary endpoint addressed intraindividual comparison of BrM thickness in treated versus untreated fellow eyes. TS-R power titration in the retinal periphery produced barely visible spots at 10.5 mW  $\pm$  2.0. Power was then reduced by 70% to a mean of 3.8 mW  $\pm$  1.4. A mean of 91.5  $\pm$  9 spots was placed uniformly across the optic disc centered approximately 50° field of view fundus (see Fig. 2). TEM revealed a significant reduction of BrM

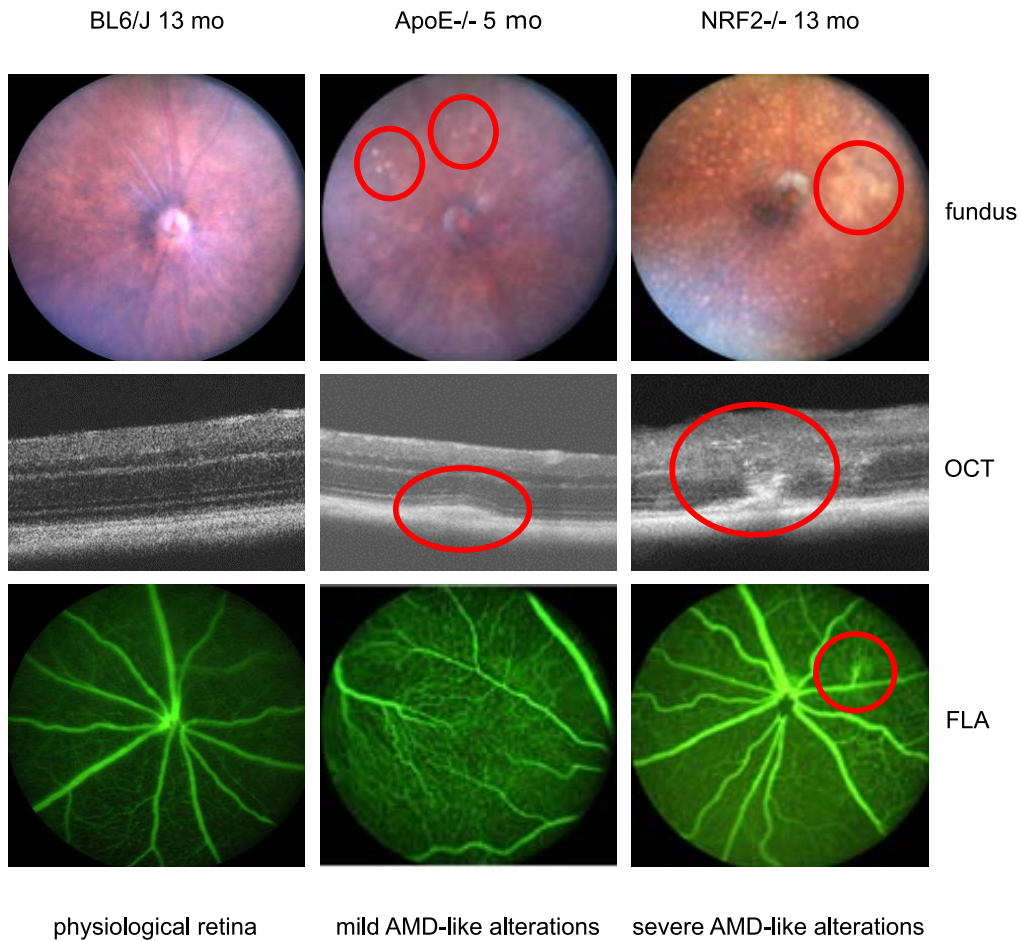


**Figure 3.** Fundus images, OCT, and FLA examinations showed a physiological phenotype in all BL/6J wild type control mice (*left column*). Most ApoE<sup>-/-</sup> had mild AMD-like alterations like DRS in fundus images and OCT (*middle column red encircled*). Those alterations could not be seen in FLA. NRF2<sup>-/-</sup> mice generally had a more severe AMD-like phenotype with many DRS and pigment alterations and even CNV formation in one eye (*right column, red encircled*).

thickness in 18/19 laser treated eyes (one mouse died preterm) compared to their fellow control eyes ( $P < 0.0001$ ; Fisher) 1 month after laser treatment (see Fig. 6). Five-month-old ApoE<sup>-/-</sup> control eyes had a mean BrM thickness of 586 nm  $\pm$  12.9 SEM, the TS-R laser treated fellow eye 525 nm  $\pm$  11.4 SEM ( $P = 0.0005$ ; paired  $t$ -test). Nine-month-old ApoE<sup>-/-</sup> control eyes' mean BrM thickness was 603 nm  $\pm$  12 SEM, mean BrM thickness of the TS-R laser treated fellow eyes was 527 nm  $\pm$  12 SEM ( $P < 0.0001$ ). Mean BrM thickness of 10-month-old NRF2<sup>-/-</sup> control mice was 666 nm  $\pm$  13.3 SEM, the TS-R laser treated fellow eyes had a mean BrM thickness of 598 nm  $\pm$  13.1 SEM ( $P = 0.0003$ ). Thirteen-month-old NRF2<sup>-/-</sup> control eye mean BrM thickness was 662 nm  $\pm$  12.2 SEM, laser treated fellow eyes had a mean BrM thickness of 593 nm  $\pm$  11.8 SEM ( $P < 0.0001$ ).

### Influence of TS-R on Disease Phenotype

Subthreshold TS-R laser spots were not visible by fundus imaging, OCT, and FLA, 2 hours or 1 month after laser treatment. Only threshold titration lesions were visible.

Since CRB1<sup>rd8</sup> might have influenced the clinical phenotype of NRF2<sup>-/-</sup>, DRS were counted, but not compared statistically for this strain. Only DRS found in ApoE<sup>-/-</sup> were compared statistically. There was no significant change in the number of DRS of the treated eye before TS-R compared to the treated eye after TS-R and compared to the control eyes (see Table 2). However, the fellow control eyes of 4-month-old ApoE<sup>-/-</sup> mice had a significantly increased ( $P = 0.03$ ) number of DRS when compared to 5 months of age.

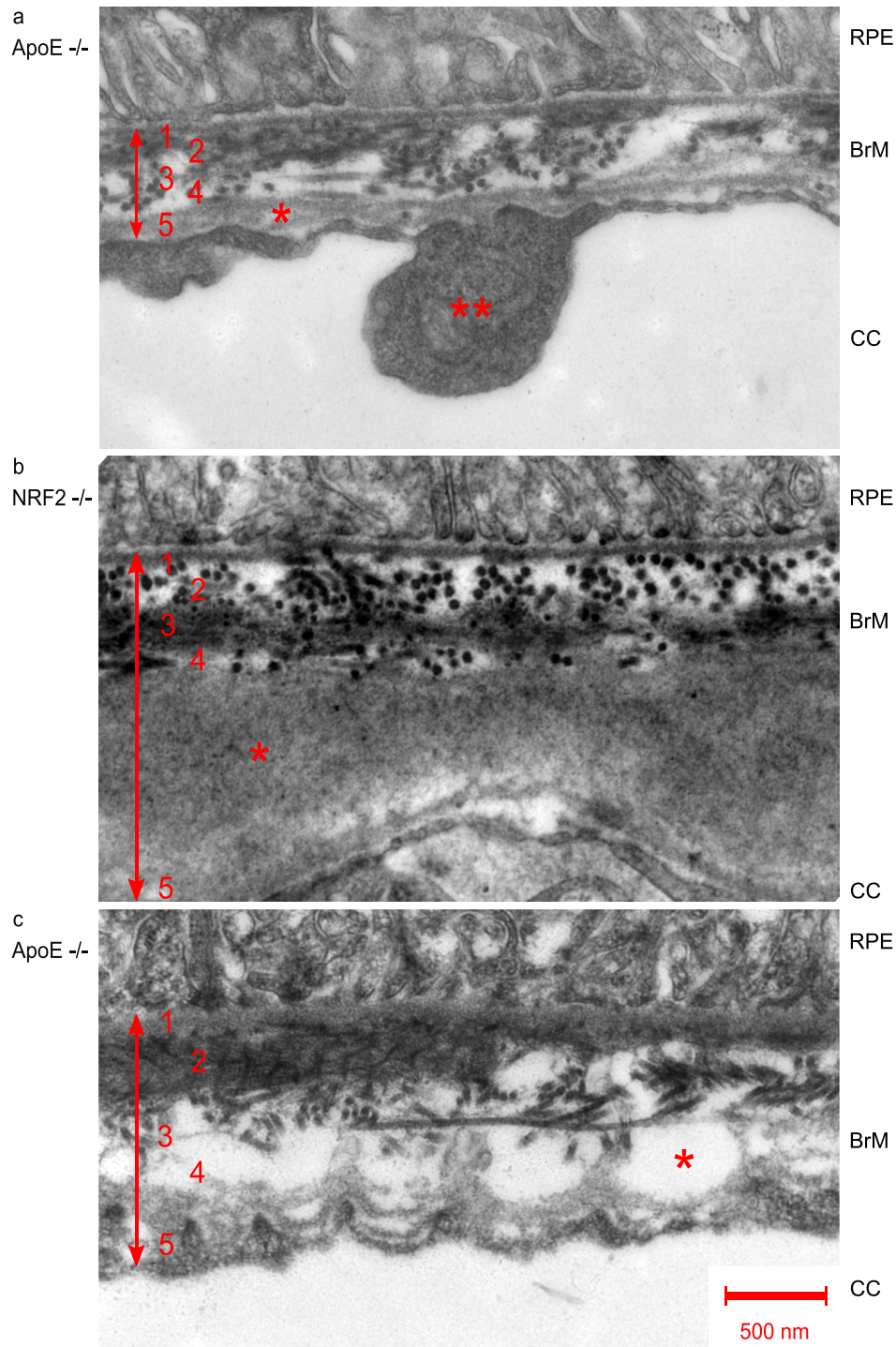


**Figure 4.** TEM (12,000-fold magnification) of RPE/BrM/choroid complex pathologies in AMD mouse models. Numbers indicate BrM layers: 1, basal lamina of RPE; 2, inner collagenous layer; 3, elastic layer; 4, outer collagenous layer; 5, basal lamina of choriocapillaris. **a** single asterisk shows basal lamina splicing, double asterisk shows endothelial thickening, both typically found in AMD, **b** asterisk indicates outer collagenous layer deposits, and **c** asterisk indicates the formation of vacuoles within the outer collagenous layer.

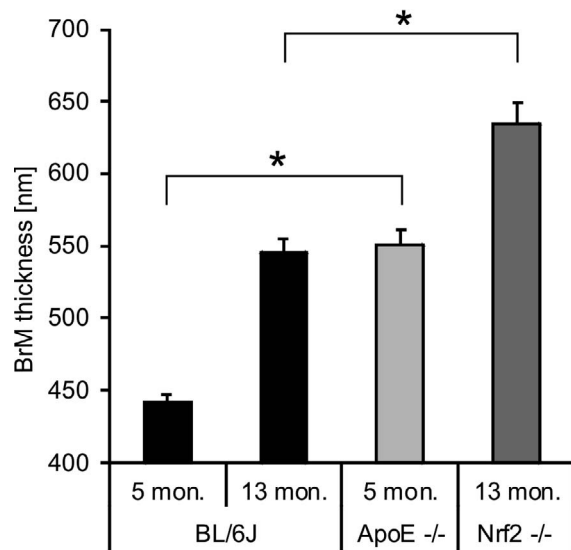


**Figure 5.** BrM thickness increases with age in wild type untreated C57BL/6J mice. Five-month-old ApoE<sup>-/-</sup> mice had a significantly increased BrM thickness compared to age-matched BL/6J mice. NRF2<sup>-/-</sup> mice also had a significantly increased BrM thickness compared to age-matched BL/6J mice. Depiction of mean + SEM. Each bar represents a total of 324 measurements from six eyes.

### Influence of TS-R on RPE Integrity and Ultrastructural Changes

RPE cells are defined as post mitotic polarized epithelial cells with apical melanosomes and long microvilli interdigitating with photoreceptor outer segments.<sup>47</sup> They have little basal pigmentation and

short basal microvilli connecting with BrM (Fig. 7B). There was no significant change between treated and untreated eyes in terms of general ultrastructural integrity in 5- and 9-month-old ApoE<sup>-/-</sup> and 10-month-old NRF2<sup>-/-</sup>. However, RPE cells with multiple vacuoles and reduced length of apical microvilli were more common ( $P=0.04$ ) in the fellow untreated eyes (10 of 12 levels, Fig. 7C) compared to TS-R treated eyes (4 of 12 levels, Fig. 7D) in 13-month-old NRF2<sup>-/-</sup> mice.

## Discussion

We present here that TS-R reduces BrM thickness, known to be pathologically enlarged in AMD. A thickened BrM leads to impaired gas and nutrient exchange, likely being one of the main causes for AMD. We hypothesize that a reduction of BrM thickness may facilitate gas and nutrient exchange and thereby prevent AMD disease progression or even cure the disease. Since neuroretina is left intact, TS-R can even be applied to critical regions of the retina, like macula and could therefore be used as an early treatment for AMD.

Both the ApoE<sup>-/-</sup> and NRF2<sup>-/-</sup> mouse models are adequate for the study of AMD therapies, since both models show a thickened BrM with AMD-like ultrastructural BrM alterations. Also, the clinical phenotype mimics AMD with DRS and pigment alterations. With ApoE<sup>-/-</sup> mice reflecting the hyper-

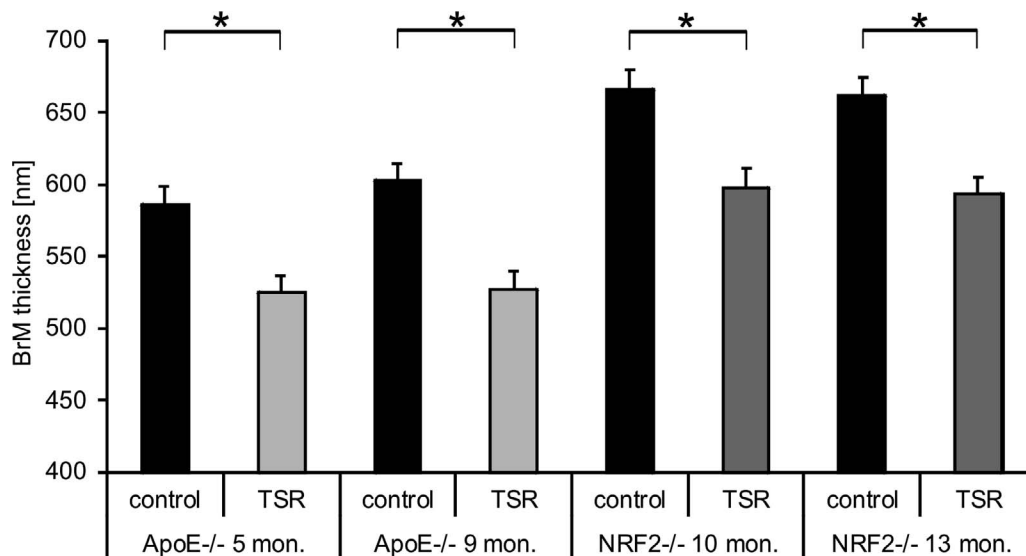


**Figure 6.** BrM thickness of the TS-R laser treated eyes (grey column) was significantly thinner than BrM thickness of the fellow untreated control eyes (black column) in all treatment groups. Depiction of the mean + SEM. Each bar represents 270 measurements from five eyes, except for the 13-month-old NRF2<sup>-/-</sup> (216 measurements) where one animal died preterm.

**Table 2.** Number of DRS Counted Within an Optic Disc Centered Fundus Image

	DRS Pretreated, <i>n</i>	DRS Posttreated, <i>n</i>	DRS Prefellow, <i>n</i>	DRS Postfellow, <i>n</i>
ApoE <sup>-/-</sup> 4 mo	4 +/- 4	7 +/- 3	<b>1 +/- 2</b>	<b>5 +/- 2</b>
ApoE <sup>-/-</sup> 8 mo	3 +/- 5	5 +/- 5	5 +/- 5	8 +/- 8
NRF2 <sup>-/-</sup> 9 mo	29 +/- 25	34 +/- 31	25 +/- 60	34 +/- 56
NRF2 <sup>-/-</sup> 12 mo	31 +/- 28	26 +/- 29	22 +/- 18	25 +/- 19

There were no significant differences between the number of DRS before laser treatment compared to 1 month after treatment. However, in the ApoE<sup>-/-</sup> 4-month-old fellow control eyes (bold letters), the number of DRS was significantly ( $P = 0.03$ ) increased 1 month after treatment (5 months of age) compared to the number of DRS before treatment.

lipidemic/hyperlipoproteinemic western lifestyle and with NRF2<sup>-/-</sup> reflecting increased oxidative stress, two of the main driving factors of AMD are present in our models. These two models together include all four main assumptions underlying the pathomechanism of AMD, altered lipid metabolism, changes of the extracellular matrix, inflammation, and altered angiogenesis. Our examinations allow for a statement on the effect of TS-R on lipid metabolism deposits (like drusen) and extracellular matrix. Angiogenesis and inflammation were not in the focus of the study. The interpretation of phenotypical AMD-like retinal

alterations may be confound by CRB1<sup>rd8</sup>. It is known that this mutation mimics AMD-like pathology clinically, for example by an abundance of DRS.<sup>48,49</sup> CRB1<sup>rd8</sup> linked DRS are neuroretinal lesions and not, like in AMD, lesions within the RPE/BrM/choroid complex. This mutation is common in BL/6N background and uncommon in BL/6J background.<sup>48,50</sup> Since both strains used in this experimental setting are created on BL/6J background, we did not expect to find CRB1<sup>rd8</sup>. However, our analysis showed that all NRF2<sup>-/-</sup> had a homozygous CRB1<sup>rd8</sup> mutation, none of the other strains were

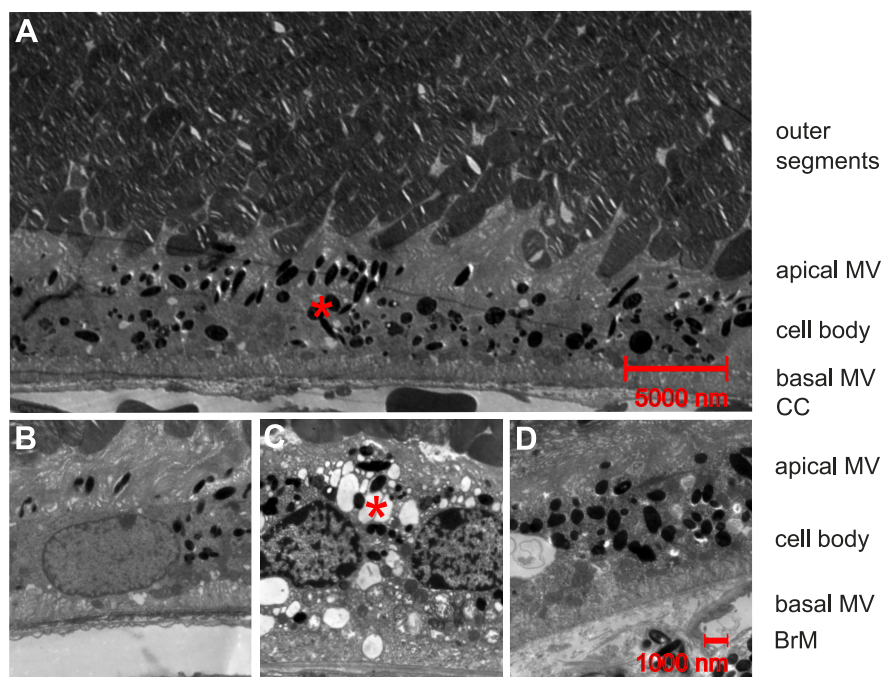


**Figure 7.** Ultrastructural anatomy of RPE cells. (A) 1100-fold magnification of a TS-R lasered 5-month-old ApoE<sup>-/-</sup> eye 1 month after treatment showing physiological anatomy. Photoreceptor outer segments interdigitate with long apical microvilli (MV) of RPE cells. Melanosomes (red asterisk) are more common in apical MV and apical cell body. Basal microvilli are free of melanosomes and connect with BrM. Choriocapillaris (CC) is located posterior to BrM. (B) 3000-fold magnification of a TS-R lasered 5-month-old ApoE<sup>-/-</sup> eye 1 month after treatment showing physiological anatomy. (C) 3000-fold magnification of the untreated fellow control eye of a TS-R lasered 1-month-old NRF2<sup>-/-</sup> eye 1 month after treatment. Multiple vacuoles (red asterisk) within the RPE cell and a reduced number and length of apical microvilli can be seen. (D) 3000-fold magnification of the TS-R treated eye of C showing physiological anatomy.

affected. The experiments conducted here are translational with focus on BrM thickness. The AMD-like pathology of the RPE/BrM/choroid complex should not be affected by CRB1<sup>rd8</sup>. Changes due to the mutation are expected within neuroretinal layers. It may though affect the clinical phenotype. Indeed, the variability and in some individuals the abundance of DRS in NRF2<sup>-/-</sup> suggests CRB1<sup>rd8</sup> involvement (Fig. 3). To exclude any confounder, DRS count in NRF2<sup>-/-</sup> mice was excluded from statistical analysis. CRB1<sup>rd8</sup> is unlikely to be a confounder concerning the primary endpoint of the study.

We can clearly demonstrate that TS-R leads to BrM thickness reduction in both AMD mouse models, independently of age, providing evidence for the efficacy of the treatment, even after one laser session. The pilot study presented here cannot make any statement concerning dose-response relations. This analysis needs to be done in future studies.

Besides the above described influence on BrM thickness as primary endpoint, we also examined the effect of TS-R on the phenotype of AMD-like alterations in our mouse models as secondary endpoint. We did not see any influence of the single TS-R treatment on clinically visible AMD-like alterations in the ApoE<sup>-/-</sup> model. However, 4-month-old ApoE<sup>-/-</sup> fellow control eyes had a significant increase in the number of DRS, their fellow treated eyes did not show that increment. This might indicate that TS-R inhibits drusen formation in treated eyes. One must be careful with this statement though, since experimental groups are small, standard deviation is large, and the number of DRS only reflects the secondary endpoint of this pilot trial.

Ultrastructural changes of the RPE generally did not differ between TS-R lasered and untreated fellow control eyes in three of four groups. In 13-month-old NRF2<sup>-/-</sup> mice, there was a significant reduction of ultrastructural pathology in TS-R treated eyes compared to the untreated fellow eyes. TS-R might therefore be beneficial to RPE cells. Statistical analysis must be seen critical though, since focus was put on BrM thickness irrespectively of RPE display. More research on this issue to determine the effect of TS-R on RPE vitality is needed and promising based on the presented data. A harmful effect of TS-R on RPE cells seems very unlikely and can likely be excluded.

Currently there is no adequate treatment for early AMD. The effect of dietary supplements, such as the AREDS formula, for an inhibition of disease progression or even as preventive measure is contro-

versially discussed and has not been shown to stop legal blindness following end-stage dry AMD.<sup>50-52</sup> Current research is focused on the specific treatment of certain parts of AMD molecular mechanisms. Single drusen components,<sup>53,54</sup> complement,<sup>53</sup> and oxidative processes<sup>55</sup> are such targets. So far, none of the current concepts have proven success in treating AMD. This might be due to the limited focus on single players within the orchestra of molecular AMD changes. The molecular mechanisms interdigitate, hence altering only one aspect might not lead to a cure of the disease.

Laser modalities that induce hyperthermia to RPE cells or selectively disrupt these cells without damage to the neuroretina are known to induce various cell protective and regenerative mechanisms. Thermal stimulation addresses at least three of the four main assumptions underlying AMD pathomechanism. In porcine RPE/BrM/choroid organ cultures TS-R induces MMP secretion as latent enzymes<sup>55</sup> with intracellular or membrane-associated activation preforms to fully active enzymes.<sup>56</sup> Active enzymes can degrade all components of extracellular matrix, which stimulates cell migration and matrix turnover.<sup>57</sup> This could lead to a reduction of BrM thickness. Thermal stimulation induces the protective chaperones heat shock proteins (HSP)<sup>58,59</sup> in rabbit models. HSPs not only prevent cells from apoptosis by protein refolding mechanisms, but also induce anti-inflammatory processes.<sup>60</sup> A moderate temperature increase to a maximum temperature of 43°C induces antioxidant cell-protection mechanisms increasing the reduced glutathione (GSH)/oxidized glutathione (GSSG) ratio in RPE cell cultures.<sup>61</sup> TS-R reduces VEGF expression and induces PEDF expression leading to an antiangiogenic milieu (Richert E, et al. *IOVS*. 2016;57:ARVO E-Abstract 4442). It is unknown whether thermal stimulation affects lipid metabolism. The above-mentioned mechanisms have been investigated in healthy organisms. It is unknown to what extent AMD pathomechanisms are addressed by TS-R in disease. The molecular mechanisms of TS-R should be assessed further.

TS-R has not shown clinical efficacy in AMD yet. It is for the above-mentioned molecular changes induced by TS-R and based on the data presented here—a promising preventive or therapeutic approach for AMD treatment. A major concern though is the reliability of the nondamaging character. Especially if TS-R is considered a preventive measure in the critical macular region, the safety of treatment is of utmost importance. A temperature of approximately 45°C

should likely be the goal to create the wanted biological effect, without cell damage. Spot size in this study was fixed to 50  $\mu\text{m}$ , due to fiber size and laser-injector device. However, since future treatment is aimed for the macula, a small spot size is reasonable to enable a well-controlled application of laser spots in proximity to the fovea region. Also, divergent power within a spot due to the speckle pattern is reduced to a minimum within small spots enabling a homogenous distribution of power within a spot. Irradiation time was fixed to 10 ms. The Arrhenius integral<sup>57</sup> suggests that overall tissue damage is an integration of temperature over irradiation time. Hence, to reliably reach a desired degree of damage (for TS-R a temperature increase without damage is wanted) one must reach a certain temperature integral for a given irradiation time. The impact of inter- and intraindividual variances in pigmentation, optical media, and alignment on the extend of laser-induced temperature increase within RPE cells and adjacent tissue is the bigger, the longer a certain temperature curve has to be maintained. Therefore, cw laser irradiation time was reduced to a minimum of 10 ms. Following this, laser effect titration was only determined by power, controlled clinically by fundus imaging to detect retinal whitening and controlled by OCT to detect structural changes within the retina. This individual titration accounts for the general nature of optical media and species. An individual automatic dosimetry for mice that accounts for intraindividual changes in fundus pigmentation, optical media, and alignment for every spot is not available and would be difficult to obtain due to the size of a murine eye. Functional testing, like electroretinogram, has not been obtained. This would be a valuable examination for future studies not only to evaluate safety.

Barely visible retinal burns are expected to develop just over 60°C.<sup>62–65</sup> This taken, the treatment temperature we achieved after power reduction by 70% was approximately 45.2°C, with uncertainty concerning intraindividual variations. Retinal whitening or structural alterations in OCT imaging were only seen in titration areas and never detected in the treatment areas, thus assuring the nondestructive character. For patient treatment, the best evaluated laser power titration system is Endpoint Management.<sup>40</sup> Power is reduced to 30% of the last instantly visible laser spot lesion by an Arrhenius curve based algorithm. This titration modality, however, does not recognize intraindividual topic changes in light absorption capacity leading to possible over- or undertreatment.

Other dosimetry systems, like optoacoustic feedback mechanisms titrating each laser spot during the laser treatment, have been investigated experimentally in rabbits and humans with good results.<sup>66,67</sup> The only laser therapy that does not affect neuroretina, at least anatomically, known to influence AMD-like alterations in humans is 2RT™. A phase 3 clinical trial is underway. The effects on the choroid/BrM/RPE/neuroretina complex are similar to the effects we see in TS-R, except for the intended RPE cell death.

The limitations of this study are the small number of animals and the lack of knowledge concerning the number of treatments needed, the timing of the treatment, and technical treatment parameters. The laser treatment was carried out once and BrM thickness was determined 1 month after treatment. From organ culture laser experiments<sup>56</sup> (Richert E, et al. *IOVS*. 2016;57:ARVO E-Abstract 4442) we know that cell mediator levels are altered during the first days after treatment. It is unknown whether the induction of BrM altering MMP lasts even longer. We hypothesized that a possible effect on BrM might need time to develop. We therefore chose the examination time point of 1 month after TS-R. The presented data cannot give any understanding of the long-term course of disease after treatment, since we only examined at one time-point after treatment. Mouse models have general limitations. Murine eyes do not have a macula, while the anatomical structure of the retina is very similar to human retinal anatomy. And finally, there are no human clinical data on TS-R for the treatment of AMD, although TS-R has shown an effect on other retinal disease, for example, central serous retinopathy, and it proved to be safe in humans.

Despite these limitations, TS-R is a promising therapeutic approach and is worthy of further research.

## Conclusion

We conclude that TS-R leads to a reduction of pathologically increased BrM thickness in AMD, possibly by the induction of active MMPs. TS-R has the potential to be a novel and safe prophylactic or even therapeutic option for early AMD.

## Acknowledgments

The authors thank Serap Luick, Andrea Hethke, Kathrin Masur, and Frank Lichte for their excellent technical support.

This work was supported by the German Ministry of Education and Research (BMBF): Grant 13GW0043D.

An abstract of this manuscript “Laser Thermal Stimulation of the Retina (TS-R) reduces Thickness of Bruch’s Membrane (BrM) in Apolipoprotein (Apo) E knock out Mice” has been presented at the annual ARVO meeting 2016 in Seattle, WA, USA. *Invest Ophthalmol Vis Sci.* 2016;57(12):4424.

Disclosure: **J. Tode**, None; **E. Richert**, None; **S. Koinzer**, None; **A. Klettner**, None; **C. von der Burchard**, None; **R. Brinkmann**, None; **R. Lucius**, None; **J. Roider**, None

\*JT and ER contributed equally to this work.

## References

1. Klein R, Klein BE, Linton KL. Prevalence of age-related maculopathy. The Beaver Dam Eye Study. *Ophthalmology.* 1992;99:933–943.
2. Schrader WF. [Age-related macular degeneration: a socioeconomic time bomb in our aging society]. *Ophthalmol Z Dtsch Ophthalmol Ges.* 2006;103:742–748.
3. Okubo A, Rosa RH Jr, Bunce CV, et al. The relationships of age changes in retinal pigment epithelium and Bruch’s membrane. *Invest Ophthalmol Vis Sci.* 1999;40:443–449.
4. CATT Research Group,DF, Martin Maguire MG, et al. Ranibizumab and bevacizumab for neovascular age-related macular degeneration. *N Engl J Med.* 2011;364:1897–1908.
5. Fritsche LG, Igl W, Bailey JN, et al. A large genome-wide association study of age-related macular degeneration highlights contributions of rare and common variants. *Nat Genet.* 2016;48:134–143.
6. Hyman L, Neborsky R. Risk factors for age-related macular degeneration: an update. *Curr Opin Ophthalmol.* 2002;13:171–175.
7. Curcio CA, Johnson M, Rudolf M, Huang J-D. The oil spill in ageing Bruch membrane. *Br J Ophthalmol.* 2011;95:1638–1645.
8. Alexander JP, Bradley JM, Gabourel JD, Acott TS. Expression of matrix metalloproteinases and inhibitor by human retinal pigment epithelium. *Invest Ophthalmol Vis Sci.* 1990;31:2520–2528.
9. Guo L, Hussain AA, Limb GA, Marshall J. Age-dependent variation in metalloproteinase activity of isolated human Bruch’s membrane and choroid. *Invest Ophthalmol Vis Sci.* 1999;40:2676–2682.
10. Padgett LC, Lui G-M, Werb Z, Lavail MM. Matrix metalloproteinase-2 and tissue inhibitor of metalloproteinase-1 in the retinal pigment epithelium and interphotoreceptor matrix: vectorial secretion and regulation. *Exp Eye Res.* 1997;64:927–938.
11. Vranka JA, Johnson E, Zhu X, et al. Discrete expression and distribution pattern of TIMP-3 in the human retina and choroid. *Curr Eye Res.* 1997;16:102–110.
12. Parmeggiani F, Sorrentino FS, Romano MR, et al. Mechanism of inflammation in age-related macular degeneration: an up-to-date on genetic landmarks. *Mediators Inflamm.* 2013; e435607.
13. Spaide RF, Ho-Spaide WC, Browne RW, Armstrong D. Characterization of peroxidized lipids in Bruch’s membrane. *Retina Phila Pa.* 1999;19:141–147.
14. van Lookeren Campagne M, Strauss EC, Yaspan BL. Age-related macular degeneration: complement in action. *Immunobiology.* 2016;221:733–739.
15. Cherepanoff S, McMenamin P, Gillies MC, Kettle E, Sarks SH. Bruch’s membrane and choroidal macrophages in early and advanced age-related macular degeneration. *Br J Ophthalmol.* 2010;94:918–925.
16. Doyle SL, Campbell M, Ozaki E, et al. NLRP3 has a protective role in age-related macular degeneration through the induction of IL-18 by drusen components. *Nat Med.* 2012;18:791–798.
17. Segal AW. How neutrophils kill microbes. *Annu Rev Immunol.* 2005;23:197–223.
18. Wang L, Clark ME, Crossman DK, et al. Abundant lipid and protein components of drusen. *PLoS One.* 2010;5:e10329.
19. Gu X, Meer SG, Miyagi M, et al. Carboxyethylpyrrole protein adducts and autoantibodies, biomarkers for age-related macular degeneration. *J Biol Chem.* 2003;278:42027–42035.
20. Bhutto IA, McLeod DS, Hasegawa T, et al. Pigment epithelium-derived factor (PEDF) and vascular endothelial growth factor (VEGF) in aged human choroid and eyes with age-related macular degeneration. *Exp Eye Res.* 2006;82:99–110.
21. Pons M, Marin-Castaño ME. Nicotine increases the VEGF/PEDF ratio in retinal pigment epithelium: a possible mechanism for CNV in passive smokers with AMD. *Invest Ophthalmol Vis Sci.* 2011;52:3842–3853.

22. West XZ, Malinin NL, Merkulova AA, et al. Oxidative stress induces angiogenesis by activating TLR2 with novel endogenous ligands. *Nature*. 2010;467:972–976.
23. Parodi MB, Virgili G, Evans JR. Laser treatment of drusen to prevent progression to advanced age-related macular degeneration. *Cochrane Database Syst Rev*. 2009; CD006537. doi:10.1002/14651858.CD006537.pub2
24. Friberg TR, Brennen PM, Freeman WR, Musch DC, PTAMD Study Group. Prophylactic treatment of age-related macular degeneration report number 2: 810-nanometer laser to eyes with drusen: bilaterally eligible patients. *Ophthalmic Surg Lasers Imaging*. 2009;40:530–538.
25. Friberg TR, Musch DC, Lim JJ, et al. Prophylactic treatment of age-related macular degeneration report number 1: 810-nanometer laser to eyes with drusen. Unilaterally eligible patients. *Ophthalmology*. 2006; 113:622.e1.
26. Brinkmann R, Roeder J, Birngruber R. Selective retina therapy (SRT): a review on methods, techniques, preclinical and first clinical results. *Bull Société Belge Ophtalmol*. 2006:51–69.
27. Elsner H, Porksen E, Klatt C, et al. Selective retina therapy in patients with central serous chorioretinopathy. *Graefes Arch Clin Exp Ophthalmol*. 2006;244:1638–1645.
28. Roeder J, Liew SH, Klatt C, et al. Selective retina therapy (SRT) for clinically significant diabetic macular edema. *Graefes Arch Clin Exp Ophthalmol*. 2010;248:1263–1272.
29. Roeder J, Michaud NA, Flotte TJ, Birngruber R. Response of the retinal pigment epithelium to selective photocoagulation. *Arch Ophthalmol*. 1992;110:1786–1792.
30. Brinkmann R, Huttmann G, Rogener J, et al. Origin of retinal pigment epithelium cell damage by pulsed laser irradiance in the nanosecond to microsecond time regimen. *Lasers Surg Med*. 2000;27:451–464.
31. Neumann J, Brinkmann R. Boiling nucleation on melanosomes and microbeads transiently heated by nanosecond and microsecond laser pulses. *J Biomed Opt*. 2005;10:024001.
32. Richert E, Klettner AK, Koinzer SOJ, Roeder J, Hillenkamp J. Release of different cell mediators during retinal pigment epithelium (RPE) wound healing after Selective Retina Therapy (SRT) for prevention of early age-related macular degeneration (AMD). *Invest Ophthalmol Vis Sci*. 2015;56:198–198.
33. Roeder J, Liew SH, Klatt C, et al. Selective retina therapy (SRT) for clinically significant diabetic macular edema. *Graefes Arch Clin Exp Ophthalmol*. 2010;248:1263–1272.
34. Jobling AI, Guymer RH, Vessey KA, et al. Nanosecond laser therapy reverses pathologic and molecular changes in age-related macular degeneration without retinal damage. *FASEB J*. 2015;29:696–710.
35. Guymer RH, Brassington KH, Dimitrov P, et al. Nanosecond-laser application in intermediate AMD: 12-month results of fundus appearance and macular function. *Clin Experiment Ophthalmol*. 2014;42:466–479.
36. Mainster MA, Reichel E. Transpupillary thermotherapy for age-related macular degeneration: long-pulse photocoagulation, apoptosis, and heat shock proteins. *Ophthalmic Surg Lasers*. 2000;31:359–373.
37. Newsom R, McAlister J, Saeed M, McHugh J. Transpupillary thermotherapy (TTT) for the treatment of choroidal neovascularisation. *Br J Ophthalmol*. 2001;85:173–178.
38. Benner JD, Ahuja RM, Butler JW. Macular infarction after transpupillary thermotherapy for subfoveal choroidal neovascularization in age-related macular degeneration. *Am J Ophthalmol*. 2002;134:765–768.
39. Lavinsky D, Palanker D. Nondamaging photothermal therapy for the retina: initial clinical experience with chronic central serous retinopathy. *Retina Phila Pa*. 2015;35:213–222.
40. Lavinsky D, Sramek C, Wang J, et al. Subvisible retinal laser therapy: titration algorithm and tissue response. *Retina Phila Pa*. 2014;34:87–97.
41. Lavinsky D, Wang J, Hule P, et al. Nondamaging retinal laser therapy: rationale and applications to the macula. *Invest Ophthalmol Vis Sci*. 2016;57:2488–2500.
42. Ahir A, Guo L, Hussain AA, Marshall J. Expression of metalloproteinases from human retinal pigment epithelial cells and their effects on the hydraulic conductivity of Bruch's membrane. *Invest Ophthalmol Vis Sci*. 2002;43:458–465.
43. Dithmar S, Curcio CA, Le NA, Brown S, Grossniklaus HE. Ultrastructural changes in Bruch's membrane of apolipoprotein E-deficient mice. *Invest Ophthalmol Vis Sci*. 2000;41:2035–2042.
44. Zhao Z, Chen Y, Wang J, et al. Age-related retinopathy in NRF2-deficient mice. *PLoS One*. 2011;6:e19456.
45. Mulisch M, Welsch U. *Romeis - Mikroskopische Technik*. Maria Mulisch, ed. Berlin Heidelberg: Springer Spektrum; 2010.

46. Mehalow AK, Kameya S, Smith RS, et al. CRB1 is essential for external limiting membrane integrity and photoreceptor morphogenesis in the mammalian retina. *Hum Mol Genet.* 2003;12:2179–2189.
47. Strauss O. The retinal pigment epithelium in visual function. *Physiol Rev.* 2005;85:845–881.
48. Mattapallil MJ, Wawrousek EF, Chan CC, et al. The Rd8 mutation of the Crb1 gene is present in vendor lines of C57BL/6N mice and embryonic stem cells, and confounds ocular induced mutant phenotypes. *Invest Ophthalmol Vis Sci.* 2012;53:2921–2927.
49. Vessey KA, Greferath U, Jobling AI, et al. Ccl2/Cx3cr1 knockout mice have inner retinal dysfunction but are not an accelerated model of AMD. *Invest Ophthalmol Vis Sci.* 2012;53:7833–7846.
50. Aredo B, Zhang K, Chen X, et al. Differences in the distribution, phenotype and gene expression of subretinal microglia/macrophages in C57BL/6N (Crb1 rd8/rd8) versus C57BL6/J (Crb1 wt/wt) mice. *J Neuroinflammation.* 2015;12:6.
51. Age-Related Eye Disease Study Research Group. A randomized, placebo-controlled, clinical trial of high-dose supplementation with vitamins C and E and beta carotene for age-related cataract and vision loss: AREDS report no. 9. *Arch Ophthalmol.* 2001;119:1439–1452.
52. Evans JR, Lawrenson JG. A review of the evidence for dietary interventions in preventing or slowing the progression of age-related macular degeneration. *Ophthalmic Physiol Opt.* 2014;34:390–396.
53. Ambati J, Atkinson JP, Gelfand BD. Immunology of age-related macular degeneration. *Nat Rev Immunol.* 2013;13:438–451.
54. Ding J-D, Lin J, Mace BE, et al. Targeting age-related macular degeneration with Alzheimer's disease based immunotherapies: anti-amyloid-beta antibody attenuates pathologies in an age-related macular degeneration mouse model. *Vision Res.* 2008;48:339–345.
55. Broadhead GK, Grigg JR, Chang AA, McCluskey P. Dietary modification and supplementation for the treatment of age-related macular degeneration. *Nutr Rev.* 2015;73:448–462.
56. Treumer F, Klettner A, Baltz J, et al. Vectorial release of matrix metalloproteinases (MMPs) from porcine RPE-choroid explants following selective retina therapy (SRT): towards slowing the macular ageing process. *Exp Eye Res.* 2012;97:63–72.
57. Woessner JF. Matrix metalloproteinases and their inhibitors in connective tissue remodeling. *FASEB J.* 1991;5:2145–2154.
58. Sternlicht MD, Werb Z. How matrix metalloproteinases regulate cell behavior. *Annu Rev Cell Dev Biol.* 2001;17:463–516.
59. Sramek C, Mackanos M, Spitler R, et al. Non-damaging retinal phototherapy: dynamic range of heat shock protein expression. *Invest Ophthalmol Vis Sci.* 2011;52:1780–1787.
60. Yenari MA, Liu J, Zheng Z, et al. Antiapoptotic and anti-inflammatory mechanisms of heat-shock protein protection. *Ann N Y Acad Sci.* 2005;1053:74–83.
61. Iwami H, Pruessner J, Shiraki K, Brinkmann R, Miura Y. Protective effect of a laser-induced sublethal temperature rise on RPE cells from oxidative stress. *Exp Eye Res.* 2014;124:37–47.
62. Birngruber R, Hillenkamp F, Gabel VP. Theoretical investigations of laser thermal retinal injury. *Health Phys.* 1985;48:781–796.
63. Koinzer S, Hesse C, Caliebe A, et al. Photocoagulation in rabbits: optical coherence tomographic lesion classification, wound healing reaction, and retinal temperatures. *Lasers Surg Med.* 2013;45:427–436.
64. Koinzer S, Saeger M, Hesse C, et al. Correlation with OCT and histology of photocoagulation lesions in patients and rabbits. *Acta Ophthalmol.* 2013;91:e603–e611.
65. Koinzer S, Schlott K, Portz L, et al. Correlation of temperature rise and optical coherence tomography characteristics in patient retinal photocoagulation. *J Biophotonics.* 2012;5:889–902.
66. Kandulla J, Elsner H, Birngruber R, Brinkmann R. Noninvasive optoacoustic online retinal temperature determination during continuous-wave laser irradiation. *J Biomed Opt.* 2006;11:041111.
67. Koinzer S, Schlott K, Ptaszynski L, et al. Temperature-controlled retinal photocoagulation—a step toward automated laser treatment. *Invest Ophthalmol Vis Sci.* 2012;53:3605–3614.